Sixth International Symposium on Turbulence and Shear Flow Phenomena
Seoul, Korea, 22-24 June 2009

VALIDATION AND APPLICATION OF TOMOGRAPHIC PARTICLE IMAGE VELOCIMETRY FOR LARGE SCALE CONVECTIVE AIR FLOW

Matthias Kühn*, Klaus Ehrenfried, Johannes Bosbach, Claus Wagner
Institute of Aerodynamics and Flow Technology,
German Aerospace Center (DLR)
Bunsenstraße 10, 37073 Göttingen, Germany
*matthias.kuehn@dlr.de

ABSTRACT

Tomographic Particle Image Velocimetry for large scale applications (LST-PIV) is applied to a convection cell to measure the large scale flow structures in forced convection. The technique is capable to capture the three-dimensional instantaneous flow field in a measurement volume. In order to validate the implementation of the Tomographic PIV algorithm and to demonstrate that the large scale flow structure in the convection cell can be predicted properly, the data is compared to planar PIV data.

The LST-PIV reveals the same global flow structure as with planar PIV. The *rms* value of the difference between the LST- and planar PIV data amounts to 0.0088 m/s whereas the volume averaged velocity in the measurement volume is 0.11 m/s. However, small regions exist in which the differences are as large as 0.0182 m/s. It is concluded that the larger differences between the two sets of data are mainly caused by the not yet fully converged flow statistics and to a small extend by disturbance of the inflow due to particle injection.

INTRODUCTION

A very promising approach to capture the unsteady and three-dimensional flow structures in turbulence is the recently developed Tomographic Particle Image Velocimetry (Tomographic PIV; Elsinga et al., 2006b). However, in the past this novel technique was applied only to measurement volumes of the order of ten cubic centimetres (Elsinga et al., 2006b). More recently, the applicability of the technique to large scales of the order of a cubic metre was shown (Kühn et al., 2008), which is e.g. of interest for investigations of time-dependent three-dimensional large scale flow structures in turbulent thermal and mixed convection (Ahlers et al., 2009; Kunnen et al., 2008; Niemela et al., 2001; Xia et al., 2003; Schmeling et al., 2008; Westhoff et al., 2007).

The goal of our study is to demonstrate that the spatial and temporal behaviour of this large scale flow structures in a convection cell can be investigated systematically using Tomographic PIV. Furthermore, we want to validate the implementation of our Tomographic PIV algorithm. This is done by comparing Large Scale Tomographic PIV (LST-PIV) of forced convection with a Reynolds number of 530 (based on the height of the inlet channel) in the convection cell with respective planar PIV data by Schmeling et al. (2008).

The paper is outlined as follows: At first the measurement technique and the convection cell are briefly introduced. Thereafter the LST-PIV set-up and the processing of the LST-PIV data are described. Finally, the results are compared to existing planar PIV data.

LARGE SCALE TOMOGRAPHIC PIV

In Tomographic PIV the flow is seeded with small tracer particles which are illuminated twice in a measurement volume with a well defined time delay between the illuminations. The scattered light of the tracer particles is recorded simultaneously during each illumination by a camera system consisting usually of four cameras. From the projections of the tracer particles, i.e. the camera recordings, the three-dimensional intensity distribution in the measurement volume is reconstructed by means of tomography. Further, the intensity distributions are subdivided into small interrogation volumes (IVs). In the IVs the particle displacement is obtained by calculation of the cross-correlation between subsequent reconstructed intensity distributions. Thereby the position of the maximum correlation value in the correlation volume is an indication for the particle displacement. Finally, the velocity vectors are calculated by dividing the displacements by the time between the illuminations. (Elsinga et al., 2006b)

The feasibility of Tomographic PIV for large scale applications was demonstrated by Kühn et al. (2008). The technique was applied in a test set-up with a measurement volume of 0.69 m × 0.42 m × 0.24 m. This is more than 1000 times larger than the volumes used in previous applications (see e.g. Elsinga et al., 2006b). As tracer particles Helium filled soap bubbles (HFSBs) were used. In order to check if it is possible to apply Tomographic PIV to large scales, different calibration errors were analysed. It was shown that the calibration error could be reduced down to 0.1 pixel, which is necessary for the reconstruction of the three-dimensional intensity distribution with high quality (Elsinga et al., 2006b; Wieneke, 2008). Finally, the calibration accuracy was achieved by applying the so-called volume self-calibration in an iterative manner (Wieneke, 2008).

Furthermore, one should notice that LST-PIV requires a scaling of the complete system. As a consequence certain parameters of the measurement system, which could potentially affect the accuracy, are different compared to the case of small measurement volumes.

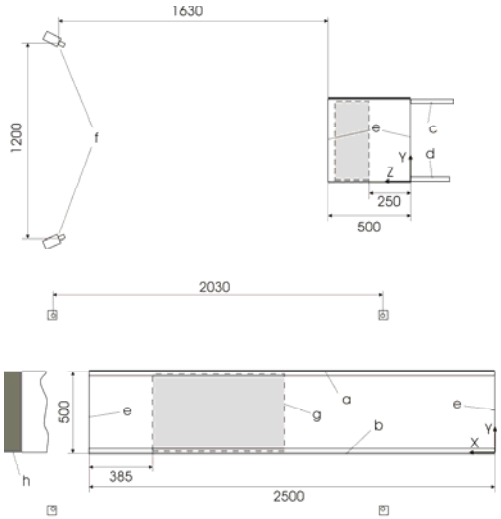

Figure 1 Schematic sketch of rectangular convection cell and LST-PIV set-up. *Y*-*Z* plane (top), *X*-*Y* plane (bottom). a – cooling plate, b – heating plate, c – air inlet, d – air outlet, e – viewports, f – cameras, g – measurement volume, h – LED light source.

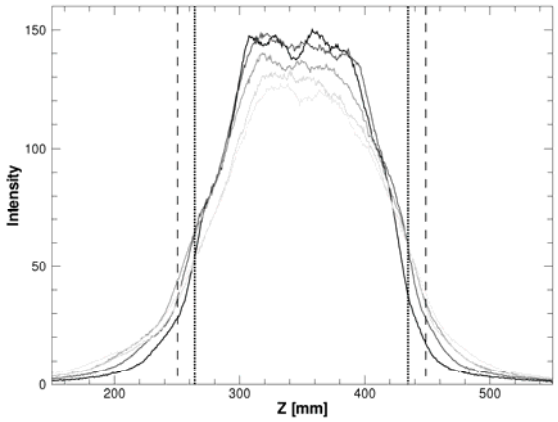

Figure 2 Intensity distribution of LED light source consisting of five 1d-LED-arrays as a function of Z at $Y \approx 250$ mm measured for different X-positions (black to light gray: $X = 2115$ mm, 1915 mm, 1715 mm, 1515 mm, 1315 mm). Dashed line indicates width of reconstructed volume and dotted line width of LED light source.

These are mainly a larger ratio between particle size and wavelength of light, and a larger ratio between particle size and voxel size. Additionally, the opening angle of the camera in the present set-up is larger.

CONVECTION CELL

A sketch of the convection cell is shown in Figure 1. The cell has a length of 2.5 m and a cross section of 0.5 m × 0.5 m. Inlet and outlet channel with a height of 25 mm and 15 mm, respectively, are attached to one side wall. By supplying air, well defined forced convection can be realized in the cell. Furthermore, in order to have a well developed inlet velocity profile the lengths of the channels equal to 30 times of the respective channel height. In order to guarantee a uniform distribution of the flow in longitudinal cell direction a settling chamber is placed in front of the inlet channel.

Moreover, a cooling plate and a heating plate are placed at the top and the bottom of the convection cell, respectively, in order to allow studies of thermal and mixed convection in the future.

Here, only forced convection is investigated. This configuration provides an ideal test case for the validation of the measurement technique since the resulting flow is statistically stationary and almost two-dimensional. Finally, the volume flow rate is set to 20.1 litres per second, which corresponds to an inlet channel Reynolds number of 530 based on the height of the channel.

MEASUREMENT SET-UP

Figure 1 provides a schematic sketch of the set-up of the LST-PIV system. The measurement volume had a size of approximately 790 mm × 450 mm × 200 mm. It was observed simultaneously by a camera system consisting of four cameras with a spatial resolution of 1392 × 1024 pixel (PCO pixelfly). Each camera was equipped with a $f = 21$ mm lens (Distagon T* 2.8/21, Carl Zeiss). The apertures were set to $f/4$. Due to the large depth of field there was no need to tilt the camera lenses relative to the image plane according to the Scheimpflug criteria. The camera viewing angles were approximately 30° and 20° in X- and Y-direction with respect to the Z-direction. According to Elsinga et al. (2006b) these inclinations provide an optimal quality in the reconstruction process.

HFSBs with a mean diameter of approximately 0.2 to 0.3 mm were used as tracer particles in the LST-PIV experiment (see Bosbach et al., 2009). In order to guarantee a homogeneous seeding density throughout the complete length of the measurement volume HFSB were injected at five different positions into the settling chamber in cell length direction. Furthermore, the HFSBs were first blown in an extra settling box of 1.5 m × 0.5 m × 0.5 m in order to homogenize the seeding. Pressurized air was used to blow the bubbles out of the box into the settling chamber. Hence approximately five percent of additional air was injected into the convection cell. Unfortunately, this method still led to a small disturbance of the velocity profile at the channel end of up to 5.5 percent with a *rms* value of 3.8 percent in longitudinal cell direction.

In order to illuminate tracer particles in a volume with defined boundaries a special LED light source was developed. The light source comprises an array of up to 225 LEDs, each having a luminous flux of 112 lm at a forward current of 350 mA. Normally, for Large Scale PIV short light pulses of several microseconds are necessary. Hence, in order to increase the brightness of the LEDs during these short pulses they are operated with a surge current of 7 A. Additionally, the length of the light pulses (500 µs in the present set-up) as well as the time between two pulses (30 ms in the present set-up) can be

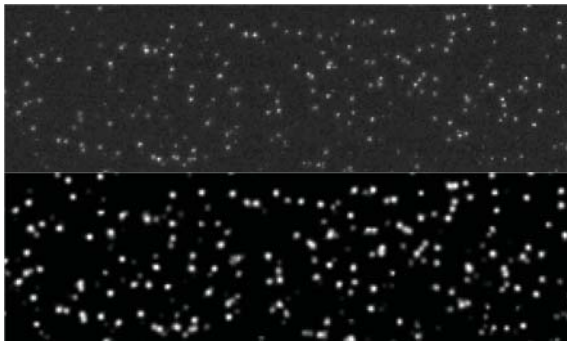

Figure 3 Projection of particle images (image section of 260 x 80 pixel). Unfiltered image (top), filtered image (bottom).

adjusted by an external TTL trigger signal making the light source suitable for PIV.

Each LED is equipped with a collimating optics consisting of a concave mirror. Furthermore, the light of a 1d-LED-array with a height of 500 mm comprising 15 LEDs is guided through a black channel in order to collimate the light resulting in a nearly parallel light beam with a remaining opening angle of approximately 2°. Hence, due to the modular arrangement of the LEDs the depth of the illuminated volume can be easily adjusted. Figure 2 provides the measured light intensity distribution from a light source consisting of five 1d-arrays as a function of the *Z*-direction at $Y = 250$ mm for five different *X*-positions. In the middle of the profile a plateau with a dimension of circa 100 mm arise. At the side of the profile the intensity decreases to 25 percent of the plateau value over a range of 50 mm, which is a result of the remaining divergence. Nevertheless, the profile could be characterised as top hat like. With increasing distance from the light source the plateau value decreases due to the remaining expansion of the light volume of the single 1d-arrays.

In order to obtain the necessary calibration function, which maps physical coordinates to image coordinates, a calibration target was traversed in *Z*-direction through the measurement volume. An image of the calibration target was recorded at five different *Z*-positions by every camera. A mapping function is obtained according to Soloff et al. (1997) by fitting third order polynomials in *X*- and *Y*-direction and a second order polynomial in *Z*-direction using the known marker positions of the calibration target (Kühn et al., 2008).

In order to increase the accuracy of the mapping for the complete camera system down to 0.1 pixel the so-called volume self-calibration is applied in an iterative manner (Wieneke, 2008). According to Elsinga et al. (2006b) and Wieneke (2008) this is necessary in order to obtain a good quality of the reconstructed intensity distribution in three-dimensional space. By the self-calibration an initial calibration error of up to 1.25 pixel per camera was decreased to an error of less than 0.05 pixel after a few iterations using $5 \times 3 \times 2$ subvolumes.

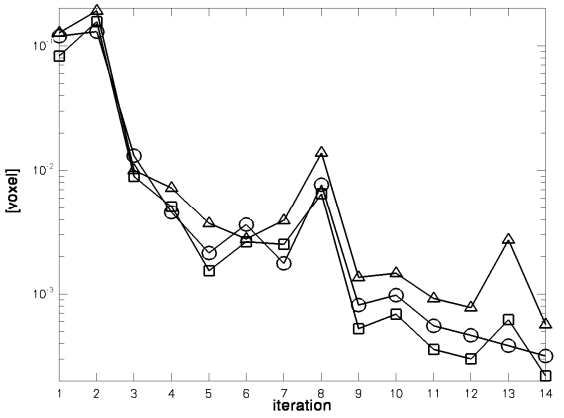

Figure 4 Average of absolute difference of displacement in *X*-, *Y*- and *Z*-direction of subsequent iterations of the reconstruction process (Δ – displacement in *X*-direction, ○ – *Y*-direction, □ – *Z*-direction). Average is calculated from values of 180 non-overlapping IVs (size of 96^3 voxel) of one instantaneous flow field.

DATA PROCESSING

During the measurement 34 instantaneous flow fields were recorded with a sampling frequency of one Hertz. The average particle density corresponds to 0.01 particle per pixel (ppp), which is relatively low for Tomographic PIV (see Elsinga et al., 2006b). As an example an image section of recorded particle images can be seen in the upper part of Figure 3. First, in order to increase the quality of the reconstructed intensity distribution, the particle projections, i.e. the camera recordings are pre-processed. The image pre-processing comprises the following steps, which are adapted by the pre-processing of Michaelis and Wieneke (2008):

- subtraction of the minimum image calculated from the complete series of recordings,
- normalisation of intensity by dividing the image by the sliding average calculated with a kernel of 51×51 pixel for the complete series of recordings,
- enlargement of particle images by applying a 3×3 Gaussian smoothing filter and
- normalisation of the particle image intensity peaks by dividing by the sliding local average (kernel size of 15×15 pixel).

In the lower part of Figure 3 the particle images after pre-processing are shown.

In order to reconstruct the three-dimensional intensity distribution in the measurement volume, the Multiplicative Algebraic Reconstruction Technique (MART; Herman and Lent, 1976; Elsinga et al., 2006b) is used. It is implemented as described in Kühn et al. (2008). The measurement volume is discretised by $975 \times 585 \times 288$ voxel. The relaxation factor μ of the MART (see equation 3 in Elsinga et al., 2006b) is set to one, the intensity distribution is initialised with ones and a bilinear interpolation filter is used. After three iterations the reconstruction is sufficiently converged. This is evidenced by the plot of the difference between the displacements in

X-, *Y*- and *Z*-direction of subsequent iterations in Figure 4. The displacements are calculated by cross-correlation of 180 non-overlapping interrogation volumes (IVs) of the reconstructed intensity distribution at two subsequent times. The size of the IVs amounts to 96^3 voxel. It is shown that the largest changes of the displacement in all directions occur between the first and the second iteration (corresponds to iteration 1 in Figure 4) and the second and the third iteration (corresponds to iteration 2 in Figure 4). The changes are of the order of a tenth to a fifth of a voxel. After the third iteration the changes in all displacement values are less than 0.015 voxel, which is approximately an order of magnitude smaller than after the first iteration. The peaks in the convergence history are mainly due to not detected outliers disturbing the average value. Nevertheless, a nearly linear trend of the plot can be recognized in the semi-log plot after the fifth iteration. Furthermore, one should notice that performing ten iterations the change of the displacement in all directions can be reduced by yet another order of magnitude compared to the result after three iterations. Anyway, one should keep in mind the calculation time which is needed for reconstruction of the three-dimensional intensity distribution.

After reconstruction two subsequent three-dimensional intensity distributions are cross-correlated using three-dimensional Fast Fourier Transformations. In order to do so IVs of 96^3, 64^3 and 48^3 voxel or 74^3, 49^3 and 37^3 mm^3 are used. Hence, each IV comprises approximately 32, 9 or 4 particles according to the particle density of 0.01 ppp. Furthermore, it should be noticed that the number of ghost particles, which potentially affect the measurement accuracy, is rather low for this seeding density. To sum up, according to Elsinga et al. (2006a) the ratio between actual particles and ghost particles is 13.6 for the present measurement.

The overlap of the IVs is set to 75 percent. Moreover, an iterative multi-pass algorithm is used. In order to detect the peak in the correlation volume with sub-pixel accuracy, one-dimensional three-point Gauss fit are applied in *X*-, *Y*- and *Z*-direction.

Details of the set-up and evaluation of the planar PIV data can be found elsewhere (Schmeling et al., 2008).

RESULTS

In Figure 5 the mean velocity field in the measurement volume obtained by averaging 34 instantaneous LST-PIV velocity fields is shown. Iso-surfaces of the velocity magnitude visualise the global structure of the flow field. Clearly, a roll like structure can be observed by the shell-like iso-surfaces. This roll structure is clearly reflected by the velocity vectors and is in good agreement with the planar PIV data provided by Schmeling et al. (2008).

The average particle displacement of the mean velocity field corresponds to 4.3 voxel, the average normalized correlation coefficient to 0.28 and the number of detected outliers is approximately 13 percent for the largest IVs (96^3 voxel).

In order to validate the implementation of the Tomographic PIV algorithm and the LST-PIV, mean velocity profiles in *Y*- and *Z*-direction are compared to

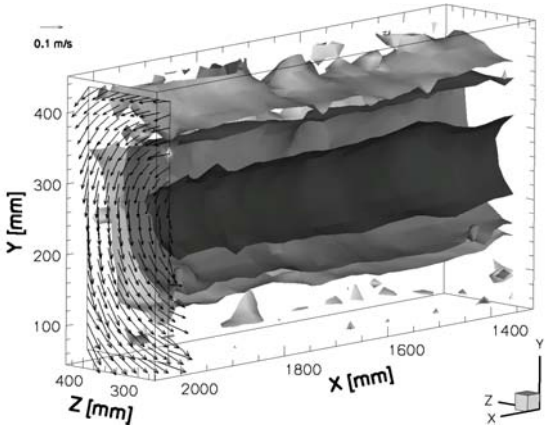

Figure 5 Overview of mean velocity field in measurement volume (average of 34 samples, IV of size of 96^3 voxel). Iso-surfaces show velocity magnitudes. Dark gray corresponds to 0.067 m/s, gray to 0.098 m/s and light gray to 0.110 m/s.

respective planar PIV data measured by Schmeling et al. (2008) at a constant *X*-position of 1562 mm.

A normalised velocity denoted by v^* is defined additionally in order to consider the accuracy of LST-PIV. v^* is normalised with the voxel size h and the separation time Δt between the recordings so that $v^* = 1$ corresponds to a particle displacement of exact one voxel.

In Figure 6 the mean velocity component in *Y*-direction is plotted as function of *Z* at $Y = 250$ mm. LST-PIV data for two different sizes of IVs and planar PIV data are compared. From both measurements a linear velocity gradient which reflects the large scale roll structure can be clearly identified. In the middle of the convection cell ($Z = 250$ mm) v_Y is close to zero. At the outer border of the measurement volume ($Z = 450$ mm) the velocity component is approximately -0.16 m/s. Considering the largest size of the IVs first, the differences of the measured velocity component are quite small between $Z = 350$ mm and $Z = 450$ mm with a maximal difference of $|\Delta v_Y^*| = 0.12$ ($|\Delta v_Y| = 0.0031$ m/s or three percent of the local velocity v_Y of planar PIV). On the other hand the difference obviously increases continuously for $Z < 350$ mm and reaches up to $|\Delta v_Y^*| = 0.65$ ($|\Delta v_Y| = 0.0167$ m/s or 65 percent at very low v_Y).

In Figure 7 the velocity component in *Z*-direction is shown as function of cell height *Y* at $Z = 350$ mm. The velocity component in *Z*-direction increases from -0.13 m/s at the bottom to 0.11 m/s at the top of the measurement volume. In the middle of the convection cell ($Y \approx 250$ mm) v_Z is zero. Comparing the LST- and planar PIV data it is observed that for $Y < 270$ mm the difference is below $|\Delta v_Z^*| = 0.13$ except for the lowest data point. Furthermore, the relative error is less than ten percent except in the region of $Y \approx 250$ mm. There the relative error is much higher due to the velocities close to zero. On the other hand for the velocity values above $Y = 270$ mm the absolute difference increases. However, with increasing *Y*, the relative difference is nearly constant with a value of 25 percent, i.e. the absolute difference increases almost linear up to $|\Delta v_Z^*| = 0.71$ ($|\Delta v_Z| = 0.0182$ m/s).

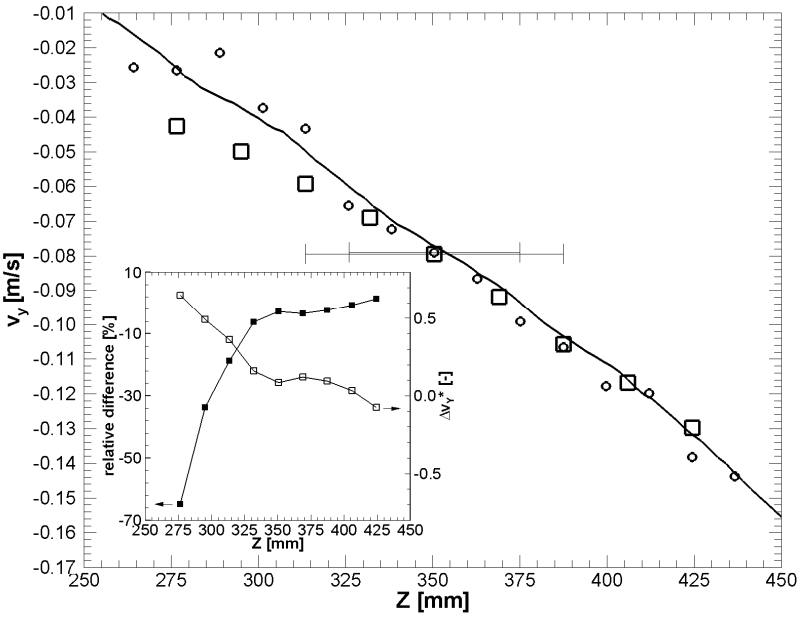

Figure 6 Mean horizontal velocity profile at $X = 1562$ mm and $Y = 250$ mm (□ – LST-PIV data, IV size of 96³ voxel, ○ – IV size of 64³ voxel; —— planar PIV data by Schmeling et al., 2008). Error bars show size of IVs. Inset shows relative difference (■) and absolute normalised difference between LST-PIV and planar PIV data (□) for IV size of 96³ voxel. Relative differences are relative to planar PIV data.

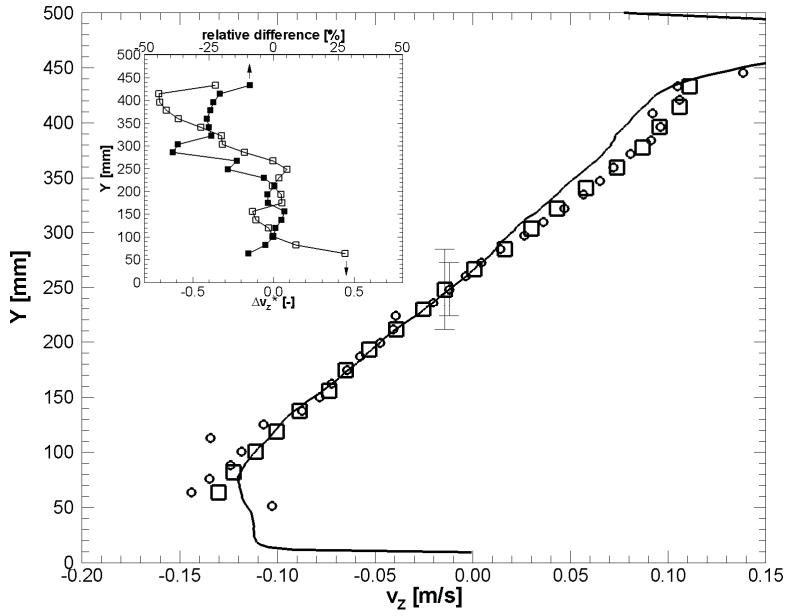

Figure 7 Mean vertical velocity profile at $X = 1562$ mm and $Z = 350$ mm (□ – LST-PIV data, IV size of 96³ voxel, ○ – IV size of 64³ voxel; —— planar PIV data by Schmeling et al., 2008). Error bars show size of IVs. Inset shows relative difference (■) and absolute normalised difference between LST-PIV and planar PIV data (□) for IV size of 96³ voxel. Relative differences are relative to planar PIV data.

As can be seen from Figure 6 and Figure 7 due to the rotational motion of the fluid an almost linear velocity gradient exists in the IVs, which could affect the PIV uncertainty and lead to additional bias errors (Westerweel, 2008). In the actual experiment the gradient amounts to 1.7 voxel particle displacement per IV (96³ voxel).

It should be noticed that the size of the IVs has little influence on the resulting Δv^* rates. In Figure 6 and Figure 7 the velocity for IVs of size 64³ voxel are presented as well. In the plot of the velocity component in Z-direction (Figure 7) nearly no difference to the largest IVs of 96³ voxel can be detected. This is also the case for the data of even smaller IVs (48³ voxel), which is omitted for the sake of visibility. However, one should notice that the profiles become noisier by decreasing the size of the IVs due to the diminishing amount of tracer particles in the IVs (see section Data Processing). On the other hand the difference between v_Z for two different size of IVs becomes larger and the difference to the planar PIV data smaller (Figure 6). Though the profile becomes noisier and no constant gradient can be identified anymore. Hence, it is very likely that the smaller difference to the planar PIV data is just effected by noise.

However, the differences between the LST- and planar PIV data are in good agreement with the findings of Elsinga et al. (2006a) in large parts of the analysed data. They have observed in their experiments that the error of Tomographic PIV is up to 0.3 voxel particle displacement (corresponds to $\Delta v^* = 0.3$) for particle densities of 0.02 to 0.08 ppp. In addition to these regions with a good match

between LST- and planar PIV data, there are regions in our measurements where the difference amounts up to $|\Delta v_Z^*| = 0.71$ ($|\Delta v_Z| = 0.018$ m/s).

It is presumed that the differences in Figure 6 arise from the fact that the flow statistic for LST-PIV is still not converged by averaging only 34 compared to 500 samples in the planar PIV rather than a result of the accuracy of Tomographic PIV. The region for $Z < 350$ mm is part of the inner core region of the convection roll, which moves instationary in the cell centre. A shift of e.g. 25 mm could already result in a change of velocity of up to 0.015 m/s, which is in the order of 50 to 100 percent in this region. Thus we are confident that by averaging over more than 34 samples the differences in this sub-domain will decrease.

On the other hand differences in the inlet velocity profiles of LST- and planar PIV measurements are observed. They are due to the additionally injected volume flow and lead to variations of the inlet velocity profiles close to the points of the particle injection. The disturbances are visible as slight bumps in the iso-surfaces of the velocity magnitude in Figure 5. As a result the global flow field could be affected. We think that this is a reason for the differences between LST- and planar PIV in Figure 7.

CONCLUSIONS AND OUTLOOK

LST-PIV is applied to a convection cell to measure the large scale flow structures in forced convection. In order to validate the implementation of the Tomographic PIV algorithm and to demonstrate that the large scale flow structure in the convection cell can be properly predicted, the data are compared to planar PIV data.

It is observed that the global flow structure is predicted in good agreement with planar PIV but in certain regions the differences between the LST- and planar PIV data amount up to $|\Delta v_Z| = 0.0182$ m/s ($|\Delta v_Z^*| = 0.71$). It is concluded that the larger differences between the two set of data are mainly caused by not yet fully converged flow statistics and to a small extend by disturbance of the inflow due to particle injection.

In future the particle injection method will be improved and the particle density will be increased. Furthermore, in order to improve the signal to noise ratio in the correlation volumes and the dynamics of the displacement an iterative volume deformation algorithm (Raffel et al., 2007; Scarano, 2002) will be implemented in the correlation algorithm.

Finally, a variation of the experimental set-up is planned in order to analyse the effects on the accuracy of LST-PIV. This includes changing the seeding density, number of cameras and thickness of light volume.

REFERENCES

Ahlers, G., Grossmann, S., and Lohse, D., 2009, "Heat transfer and large scale dynamics in turbulent Rayleigh-Bénard convection", *Reviews of Modern Physics*, in press.

Bosbach, J., Kühn, M., and Wagner, C., 2009, "Large scale particle image velocimetry with helium filled soap bubbles", *Experiments in Fluids*, Vol. 46, pp. 539-547.

Elsinga, G. E., van Oudheusden, B. W., and Scarano, F., 2006a, "Experimental assessment of tomographic-piv accuracy", *Proceedings, 13th International Symposium on Applications of Laser Techniques to Fluid Mechanics*, Lisbon.

Elsinga, G. E., Scarano, F., Wieneke, B., and van Oudheusden, B. W., 2006b, "Tomographic particle image velocimetry", *Experiments in Fluids*, Vol. 41, pp. 933-947.

Herman, G. T., and Lent, A., 1976, "Iterative reconstruction algorithms", *Computers in Biology and Medicine*, Vol. 6, pp. 273-294.

Kühn, M., Ehrenfried, K., Bosbach, J., and Wagner, C., 2008, "Feasibility study of tomographic particle image velocimetry for large scale convective air flow", *Proceedings, 14th International Symposium on Applications of Laser Techniques to Fluid Mechanics*, Lisbon.

Kunnen, R. P. J., Clercx, H. J. H., Geurts, B. J., van Bokhoven, L. J. A., Akkermans, R. A. D., and Verzicco, R., 2008, "Numerical and experimental investigation of structure-function scaling in turbulent Rayleigh-Bénard convection", *Physical Review E*, Vol. 77, pp. 016302-1-016302-13.

Michaelis, D., and Wieneke B., 2008, "Comparison between tomographic piv and stereo piv", *Proceedings, 14th International Symposium on Applications of Laser Techniques to Fluid Mechanics*, Lisbon.

Niemela, J. J., Skrbek, L., Sreenivasan, K. R., and Donnelly, R. J., 2001, "The wind in confined thermal convection", *Journal of Fluid Mechanics*, Vol. 449, pp. 169-178.

Raffel, M., Willert C. E., Wereley, S. T., and Kompenhans, J., 2007, *Particle Image Velocimetry – A Practical Guide*, Springer-Verlag, 2nd Edition.

Scarano, F., 2002, "Iterative image deformation methods in PIV", *Measurement Science and Technology*, Vol. 13, pp. R1-R19.

Schmeling, D., Westhoff, A., Kühn, M., Bosbach, J., and Wagner, C., 2008, "Flow structure formation of turbulent mixed convection in a closed rectangular cavity", *Numerical Notes on Fluid Mechanics and Multidisciplinary Design, Springer-Verlag, accepted.*

Soloff, S. M., Adrian, R. J., and Liu, Z. C., 1997, "Distortion compensation for generalized stereoscopic particle image velocimetry", *Measurement Science and Technology*, Vol. 8, pp. 1441-1454.

Westhoff, A., Grabinski, N., Bosbach, J., Wagner, C., and Thess, A., 2007, "Scaling of turbulent mixed convection under high pressure", *Proceedings, 5th International Symposium on Turbulence and Shear Flow Phenomena*, Garching.

Westerweel, J., 2008, "On velocity gradients in PIV interrogation", *Experiments in Fluids*, Vol. 44, pp. 831-842.

Wieneke, B., 2008, "Volume self-calibration for 3D particle image velocimetry", *Experiments in Fluids*, Vol. 45, pp. 549-556.

Xia, K.-Q., Sun, C., and Zhou, S.-Q., 2003, "Particle image velocimetry measurement of the velocity field in turbulent thermal convection", *Physical Review E*, Vol. 68, pp. 066303-1-066303-18.